JACS
JOURNAL OF THE AMERICAN CHEMICAL SOCIETY
Article
pubs.acs.org/JACS

Anthraquinone-Based Intramolecular Charge-Transfer Compounds: Computational Molecular Design, Thermally Activated Delayed Fluorescence, and Highly Efficient Red Electroluminescence

Qisheng Zhang,[†,§] Hirokazu Kuwabara,[†,‡,§] William J. Potscavage, Jr.,[†] Shuping Huang,[†] Yasuhiro Hatae,[†] Takumi Shibata,[†,#] and Chihaya Adachi*[,†]

[†]Center for Organic Photonics and Electronics Research (OPERA), Kyushu University, 744 Motooka, Nishi-ku, Fukuoka 819-0395, Japan

[‡]Research & Development Group, R&D Planning Division, Nippon Kayaku Company Ltd., 3-31-12 Shimo, Kita, Tokyo 115-8588, Japan

[#]Advanced Technology R&D Department, Research and Development Division, Japan Display Inc., 3300, Hayano, Mobara, Chiba 297-8622, Japan

Supporting Information

ABSTRACT: Red fluorescent molecules suffer from large, non-radiative internal conversion rates (k_{IC}) governed by the energy gap law. To design efficient red thermally activated delayed fluorescence (TADF) emitters for organic light-emitting diodes (OLEDs), a large fluorescence rate (k_F) as well as a small energy difference between the lowest singlet and triplet excited states (ΔE_{ST}) is necessary. Herein, we demonstrated that increasing the distance between donor (D) and acceptor (A) in intramolecular-charge-transfer molecules is a promising strategy for simultaneously achieving small ΔE_{ST} and large k_F. Four D-Ph-A-Ph-D-type molecules with an anthraquinone acceptor, phenyl (Ph) bridge, and various donors were designed, synthesized, and compared with corresponding D-A-D-type molecules. Yellow to red TADF was observed from all of them. The k_F and ΔE_{ST} values determined from the measurements of quantum yield and lifetime of the fluorescence and TADF components are in good agreement with those predicted by corrected time-dependent density functional theory and are approximatively proportional to the square of the cosine of the theoretical twisting angles between each subunit. However, the introduction of a Ph-bridge was found to enhance k_F without increasing ΔE_{ST}. Molecular simulation revealed a twisting and stretching motion of the N−C bond in the D-A-type molecules, which is thought to lower ΔE_{ST} and k_F but raise k_{IC}, that was experimentally confirmed in both solution and doped film. OLEDs containing D-Ph-A-Ph-D-type molecules with diphenylamine and bis(4-biphenyl)amine donors demonstrated maximum external quantum efficiencies of 12.5% and 9.0% with emission peaks at 624 and 637 nm, respectively.

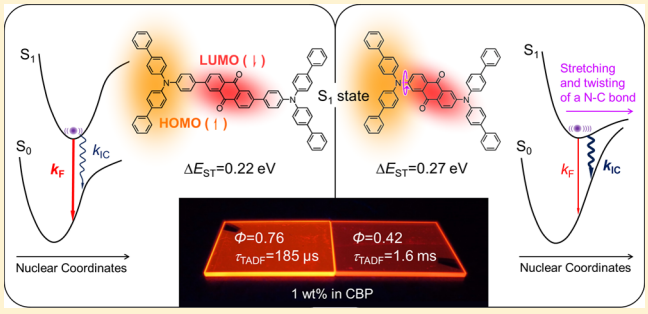

INTRODUCTION

When the energy difference between the lowest singlet (S_1) and triplet (T_1) excited states (ΔE_{ST}) is small, molecules can upconvert from the T_1 to S_1 by absorbing environmental thermal energy and then radiatively decay from the S_1 (Scheme 1). This light emission is called thermally activated delayed fluorescence (TADF). Although TADF from many-types of pure organic compounds has been reported since 1930,[1] high-efficiency and short-lifetime TADF emitters for application to organic light-emitting diodes (OLEDs) were only developed in recent years.[2] TADF emitters in OLEDs can convert triplet excitons, which constitute 75% of electrically generated excitons, into light with a theoretical yield up to 100%, which could only be realized by employing noble-metal-based phosphors and Cu(I) complexes until two years ago.[3,4] Although many efficient metal-to-ligand charge-transfer (MLCT) Cu(I) complexes also show thermally activated emission at room temperature,[4b,e,5] they are more likely an intermediate between phosphors and TADF emitters because of the mixing of ^{1}MLCT and ^{3}MLCT states by their heavy metal centers.[4d,e] Since heavy-atom-free TADF emitters are cheaper than noble-metal complexes and offer more design freedom than four-coordinate tetrahedral Cu(I) complexes, they have become a hot topic in the fields of electroluminescence (EL) and electrochemiluminescence (ECL) following in the footsteps of phosphorescent materials.[6−9]

For TADF emitters used in OLEDs, a high photoluminescence (PL) quantum yield (Φ) can enhance the upper limit of the internal EL quantum efficiency (IQE),

Received: October 2, 2014
Published: December 3, 2014

   dx.doi.org/10.1021/ja510144h | J. Am. Chem. Soc. 2014, 136, 18070−18081

Scheme 1. Jablonski Diagram for a Typical TADF Emitter[a]

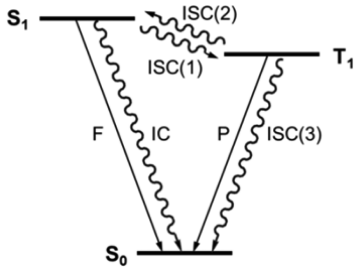

[a]Abbreviations: F, fluorescence; P, phosphorescence; IC, internal conversion; ISC, intersystem crossing. ISC represents a process from S_1 to T_1 in this paper unless stated otherwise.

while a short TADF lifetime can reduce the device efficiency roll-off caused by triplet−triplet annihilation (TTA), singlet−triplet annihilation (STA), and triplet−polaron annihilation (TPA).[10] To achieve a short natural lifetime of TADF, the rate constant of fluorescence (k_F) should be large while ΔE_{ST} should be small, with emphasis placed on the latter.[2e] On the other hand, to achieve a high Φ, k_F should be significantly higher than the rate constant (k_{IC}) of internal conversion (IC) from S_1 to S_0, and ΔE_{ST} should also be small so that the rate constant of intersystem crossing (ISC) from T_1 to S_1 can be considerably higher than that from T_1 to S_0. As we known, two conditions must be met for a small ΔE_{ST}. The first is a small exchange integral ($J_{if} = 1/2\Delta E_{ST}$) for the S_1 transition, which is roughly proportional to the orbital overlap integral ($S_{if} = \langle \phi_i | \phi_f \rangle$) between the initial ($\phi_i$) and final ($\phi_f$) state orbitals and corresponds to the degree of spatial overlap of the orbitals (page 63 in ref 11). The second is that the orbitals involved in the S_1 and T_1 transitions are not extremely different.[2b,e]

A successful approach to realizing high-efficiency and short-lifetime TADF is to create a bipolar molecule with a large dihedral angle (θ) between a N-donor and a phenyl ring substituted with electron-withdrawing groups (Scheme 2, **a**-type),[2c,e,8] which is similar to the so-called pretwisted intramolecular charge-transfer (ICT) molecules.[1c,12] In comparison with exciplex systems and quaternary carbon-linked donor−bridge−acceptor (D-B-A) systems,[6,7] pretwisted-ICT-type TADF emitters have higher k_F and Φ values owing to the partial overlap of orbitals on the phenyl ring and an approximately proportional relationship between k_F and S_{if}^2 (see eq 1).[13] ICT emitters with large dihedral angles have realized efficient blue and green TADF.[2c,e] However, the yellow and orange emitters show relatively low Φ because their k_F are not high enough to compete with k_{IC} that are increasing based on the energy gap law.[2c,e,8] Owing to the naturally small k_F of MLCT complexes, improving Φ of red Cu(I) complexes has also been a challenge for chemists in the past three decades.[14]

Scheme 2. Models for Donor−Acceptor and Donor−Bridge−Acceptor Molecules

An important design consideration for efficient red TADF is to obtain a large k_F as well as an acceptable ΔE_{ST}. The introduction of an additional aromatic bridge to increase the D/A separation distance may be a solution (Scheme 2, **b**-type). For charge-transfer (CT) transitions with weak electronic coupling, the vertical transition rate (k_V) can be described by an approximate expression based on first principles as follows:[13]

$$k_V = KE_V H_{if}^2 r^2 \quad (1)$$

where K is a constant, E_V is the transition energy, r is the effective D/A separation distance, and H_{if} is the electronic coupling (also called transfer integral) which is predicted to be proportional to S_{if} in this case.[15] Unlike for $^1CT/^3CT$ splitting, which depends mostly on S_{if},[11] k_V is related to more factors including distance r. Therefore, if two ICT molecules have similar degrees of orbital overlap (or ΔE_{ST}), the molecule with larger r will have a larger k_F.

On the basis of the previous considerations, we designed a series of symmetric D-π-A-π-D molecules with anthraquinone (AQ) as acceptor, diphenylamine (DPA), bis(4-biphenyl)amine (BBPA), 3,6-di-*tert*-butylcarbazole (DTC), and 9,9-dimethyl-9,10-dihydroacridine (DMAC) as donors, and phenyl (Ph) rings as π-bridges (Scheme 3). The selection of AQ is due to its high T_1 energy level (2.73 eV) as well as strong electron-withdrawing capability,[16] which is another key to realizing red TADF. For comparison, D-A-D-type molecules were also synthesized by directly linking the donor and acceptor units. In this paper, the influences of the D/A separation distance and the dihedral angles between subunits on the photophysical properties of these AQ-based ICT compounds are thoroughly investigated in terms of ΔE_{ST}, k_F, and k_{IC}.

Scheme 3. Molecular Structures of Compounds a1−4 and b1−4

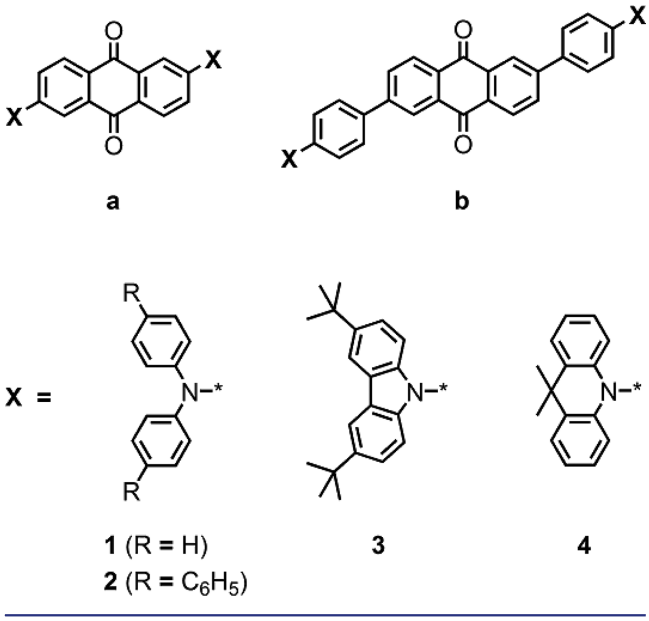

RESULTS AND DISCUSSION

Molecular Simulations. Density functional theory (DFT) and time-dependent density functional theory (TD-DFT)[17] were employed to reproduce the S_0 and S_1 geometries, respectively, of these AQ-based ICT molecules. It is known

dx.doi.org/10.1021/ja510144h | J. Am. Chem. Soc. 2014, 136, 18070−18081

that the configuration interaction (CI) description of the S_1 transition as well as the optimized geometry of the S_1 state for an ICT molecule depend on the exchange-correlation (XC) functional of TD-DFT.[18] The reason for this is that a CT state is more sensitive to the Hartree−Fock percentage (HF%) in traditional XC functionals than a locally excited state (LE),[19,20] and therefore the gap and coupling between a ^{1}CT state (S_1) and higher lying ^{1}LE states can be affected by using different XC functionals. Given that there is not much difference in CT amount (q) between the S_1 transitions based on the S_0 and S_1 geometries for these ICT molecules, optimizing S_1 geometries on the basis of a functional with a HF% close to the optimal HF % (OHF) employed for the calculation of vertical absorption energy from S_0 to S_1 ($E_{VA}(S_1)$) may minimize the error.[18b,20] Accordingly, the S_0 geometries of all studied molecules were first optimized using the B3LYP functional[21] with 6-31G(d) basis set in vacuum as an initial guess. The q was analyzed by Multiwfn,[22] and the OHF for the $E_{VA}(S_1)$ calculation was obtained by an empirical relationship of OHF = 42q (Supporting Information (SI), Table S1).[20] Then, the geometries on the S_1 state were optimized by TD-DFT with a functional with HF% close to OHF at the 6-31G(d) level in toluene.[23,24] Although S_0 geometries are generally insensitive to the XC functional and solvent, to have a better comparison, their simulation was redone in toluene by using the same methods for the corresponding S_1 geometries.

In the S_0 state, the twisting of D-π-A units in **b1**−**3** can adopt two models (Scheme 4). Model **I** is that the dihedral angle between D and A units is equal to that between the D unit and Ph-bridge (θ_1) plus that between the A unit and Ph-bridge (θ_2). Model **II** is that the dihedral angle between D and A units equals θ_1 minus θ_2. The S_0 geometry simulation of **b1** reveals the same energies for these two models, indicating an equal chance of their existence (SI, Figure S1). Here, we select model **I** for all of the following simulations. The geometries and frontier orbitals of the S_0 state for all eight molecules are shown in Figure 1, and the important geometrical parameters are listed in Table 1. The molecules based on DPA and BBPA donors have relatively small dihedral angles of 29−38° between the donors and either the AQ-acceptor (**a**-type) or the Ph-bridge (**b**-type), θ or θ_1. In contrast, the molecules based on the donor DMAC have extremely large dihedral angles of 85−90° due to the large steric hindrance.[2e] The dihedral angles of θ and θ_1 in the DTC-based molecules (46−50°) are between those of the other molecules. Note that the HOMO → LUMO transitions are all symmetry forbidden for these symmetrical molecules, while the HOMO−1 → LUMO transitions with approximate energies are allowed (SI, Table S2). Herein, the low-energy transitions predominated by the latter are regarded as the S_1 transition. As shown in Figure 1, the LUMO orbitals are localized mainly on the AQ-acceptors and slightly on the adjacent nitrogen atoms or Ph-bridges. In contrast, the HOMO−1 orbitals are mainly distributed on the donors and only partially on the adjacent Ph-bridge or AQ-acceptor. Increasing the dihedral angles θ and θ_1 inhibits the delocalization of the nitrogen lone pair to the π system of the AQ-acceptor and Ph-bridge, respectively, leading to a smaller overlap of the frontier orbitals and decreased coplanarity between Ph-bridges and the AQ-acceptor for **b**-type molecules (Table 1). Owing to the enlarged D/A separation distance, the orbital overlap of a **b**-type molecule is smaller than that of the **a**-type molecule with the same donor. Similarly, the orbital overlap of a BBPA-donor molecule is also smaller than that of the corresponding DPA-based molecule.

In the relaxed S_1 state (one electron in the HOMO and one in the LUMO), HOMO and HOMO−1 localize on different

Scheme 4. Two Twisting Models for Donor−Bridge−Acceptor Moieties

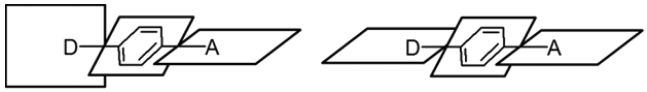

I II

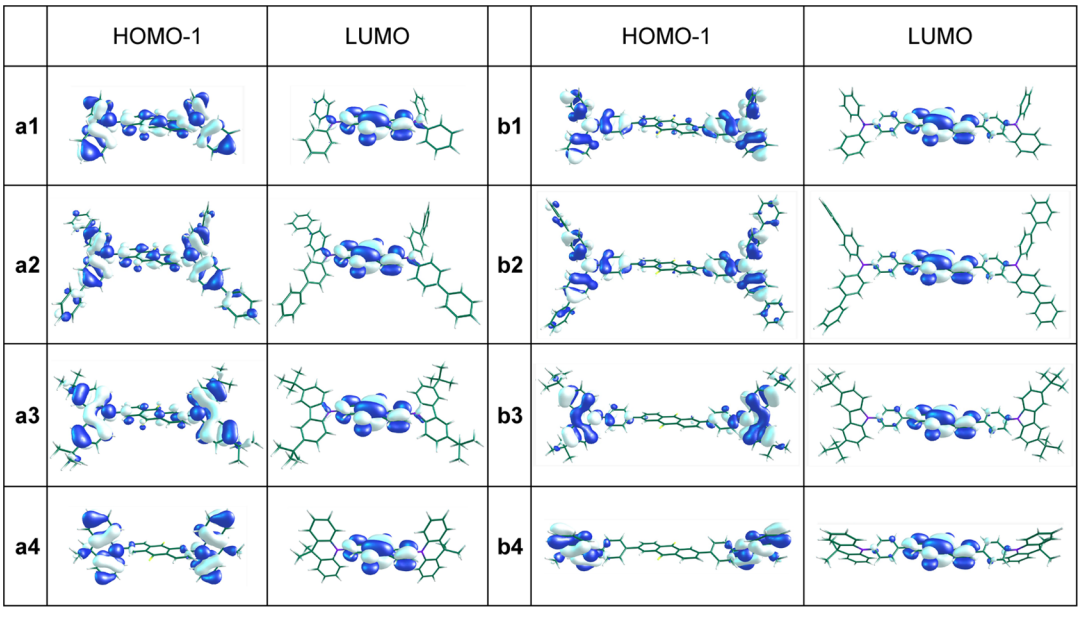

Figure 1. HOMO−1 and LUMO of the investigated molecules in their S_0 state in toluene. **a1**−**3** were optimized at the DFT/MPW1B95/6-31G(d) level,[23] while **a4** and **b1**−**4** were optimized at the DFT/BMK/6-31G(d) level.[24]

dx.doi.org/10.1021/ja510144h | J. Am. Chem. Soc. 2014, 136, 18070−18081

Table 1. Computed Twisting Angles (θ_1, θ_2, and θ), Bond Lengths (l_1, l_2, and l), Transition Energies (E_{VA} and E_{VE}, OHF Values), Exchange Energy between ^{1}CT and ^{3}CT (ΔE_{ST}(CT)), Oscillator Strengths (f_{VA} and f_{VE}, OHF Values), and Transition Rates (k_{VA} and k_{VE}) of the Investigated Molecules in Toluene on S_0 and S_1 Geometries Optimized by the Same Methods in Figures 1 and 2

	S_0 geometry in toluene						S_1 geometry in toluene					
	θ_1/θ_2 or θ (deg)	l_1/l_2 or l (Å)	$E_{VA}(S_1)$ (eV)	ΔE_{ST}(CT) (eV)	f_{VA}	k_{VA} ($\times 10^7$ s^{-1})	θ_1/θ_2 or θ (deg)	l_1/l_2 or l (Å)	$E_{VE}(S_1)$ (eV)	ΔE_{ST}(CT) (eV)	f_{VE}	k_{VE} ($\times 10^7$ s^{-1})
a1	29	1.393	2.68	0.52	0.499	23.3	47	1.423	2.09	0.36	0.087	2.47
a2	30	1.395	2.58	0.46	0.590	25.6	50	1.424	1.99	0.29	0.167	4.30
a3	46	1.398	2.64	0.29	0.353	16.0	57	1.423	2.19	0.19	0.087	2.72
a4	90	1.429	2.22	0.01	0.0001	0.003	90	1.449	1.78	0.01	0.0001	0.002
b1	34/31	1.410/1.487	2.69	0.25	0.510	24.0	36/29	1.385/1.473	2.27	0.26	0.312	10.5
b2	38/34	1.413/1.488	2.64	0.18	0.457	20.7	38/29	1.402/1.478	2.25	0.21	0.334	11.0
b3	50/36	1.412/1.490	2.92	0.12	0.255	14.2	47/29	1.404/1.479	2.49	0.16	0.195	7.87
b4	85/37	1.431/1.491	2.69	0.002	0.002	0.094	90/29	1.448/1.484	2.27	0.001	0.0001	0.003

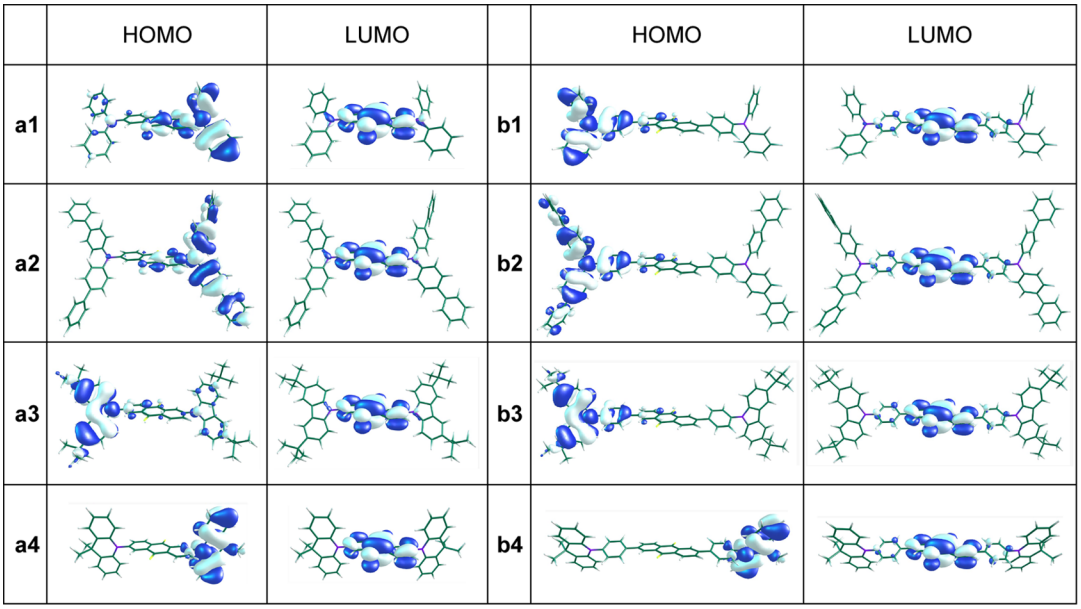

Figure 2. HOMO (one electron) and LUMO (one electron) of the investigated molecules in their S_1 state in toluene. **a1−3** optimized at the TD-DFT/MPW1B95/6-31G(d) level, while **a4** and **b1−4** were optimized at the TD-DFT/BMK/6-31G(d) level.

individual donors due to symmetry breaking (Figure 2; SI, Table S2). The transition between HOMO and LUMO becomes allowed and lowest. Thus, the excited state relaxation for each molecule will be discussed on the basis of changes on the side where the HOMO is located. In S_1, the dihedral angles θ in **a1−3** enlarge by 10−20° along with an increase in the bond lengths (l) between N-atoms and AQ-acceptors (N−C bonds) relative to the corresponding values in the S_0 state (Table 1). Such an internal rotation is somewhat like that observed in twisted ICT (TICT) molecules,[12a] and can be explained by the so-called minimum overlap rule.[25] That is, the energy of a CT state can be lowered by geometry relaxation toward a total charge separation on the donor and acceptor. Despite a few reports of the rotational relaxation of ICT molecules with large-size diphenylamine donors in polar solvents,[26] such a large-amplitude nuclear rearrangement in amorphous organic semiconductors has not yet been reported and needs to be further investigated with additional experiments. On the other hand, the behavior of **b**-type molecules in the excited state is more like that of the biphenyl-bridged D-π-A molecules that have been thoroughly studied by Maus et al.[27] In S_1, the delocalization of the excited electron on the π system of the Ph-bridge and AQ-acceptor enhance their conjugation, leading to decreased θ_2 (coplanarization) and l_2 (bond length alternation) (Table 1). The lack of a significant change in θ_1 from S_0 to relaxed S_1 may be attributed to the enlarged D/A separation distance and weak D-A electronic coupling in the Franck−Condon state.

The $E_{VA}(S_1)$ and $E_{VE}(S_1)$ (vertical emission energy) for all eight molecules were calculated in toluene by using the OHF/TD-DFT method on the basis of the optimized S_0 and S_1 geometries, respectively.[20] Because of the logarithmic relationship between the vertical transition energy and the HF% in XC functionals (HF% ≥ 20%),[2e,20] $E_{VA}(S_1)$ and $E_{VE}(S_1)$ were first calculated using the B3LYP (20% HF) and BMK (42% HF) functionals with 6-31G(d) basis set, and $E_{VA}(S_1$, OHF) and $E_{VE}(S_1$, OHF) were read from a straight line between the two transition energy−HF% points (Table S2) plotted on a log−log scale. According to the calculation, these molecules have approximate CT absorption peaks at around 460−480 nm, except for **a4** (560 nm) and **b3** (425 nm), and the energy differences of 0.4−0.6 eV between the absorption and emission maxima. In S_1, since the CI description of the T_1 transitions reproduced by TD-DFT/B3LYP is similar to that of the S_1

dx.doi.org/10.1021/ja510144h | J. Am. Chem. Soc. 2014, 136, 18070−18081

transitions (^{1}CT), the transition-energy-related ^{1}CT−^{3}CT splitting can be calculated by the following formula:[20]

$$\Delta E_{ST}(CT) = E_{VE}(S_1, OHF) - E_{VE}(T_1, B3LYP) \times E_{VE}(S_1, OHF)/E_{VE}(S_1, B3LYP) \quad (2)$$

The exchange energy between ^{1}CT and ^{3}CT transitions (HOMO−1 → LUMO) in a S_0 geometry can be calculated in the same way (Table 1). The $E_{0-0}(^1CT)$ and $E_{0-0}(^3CT)$ can then be evaluated by

$$E_{0-0}(^1CT) = [E_{VE}(S_1, OHF) + E_{VA}(S_1, OHF)]/2 \quad (3)$$

$$E_{0-0}(^3CT) = E_{0-0}(^1CT) - \Delta E_{ST}(CT) \quad (4)$$

where $\Delta E_{ST}(CT)$ is computed on the basis of the S_1 geometries. On the other hand, $E_{0-0}(^3LE)$ of all of the investigated molecules can be predicted from their $E_{VA}(T_3, B3LYP)$ (Table S2) by an experience coefficient method:[20]

$$E_{0-0}(^3LE) = E_{VA}(T_3, B3LYP)/C - \Delta E_{Stokes} \quad (5)$$

where C is a correction factor found to be 1.02 for the B3LYP functional and ΔE_{Stokes} is the Stokes-shift energy loss for a LE transition in toluene (0.07 eV) (see experimental details in the SI).

Since the calculated $E_{0-0}(^3LE)$ are all higher than or close to the $E_{0-0}(^3CT)$ (Table S1), the computed $\Delta E_{ST}(CT)$ ranging from 0.52 to 0.001 eV can be taken to be their ΔE_{ST}, which is seen to depend strongly on the degree of orbital overlap (Figures 1 and 2). At a qualitative level, if we assume that these short-range ICT have a proportional relationship between S_{if} and H_{if} like that found in long-range CT and intermolecular CT,[15] $\Delta E_{ST}(CT)$ is expected to be related to J_{if}, S_{if}, and, in turn, H_{if}. Additionally, the electronic coupling between a directly connected donor and acceptor was found to be proportional to the cosine of their dihedral angle,[27e,28] while the electronic coupling of a donor−bridge−acceptor molecule is proportional to the product of the electronic coupling of the donor and bridge and that of the bridge and acceptor via a superexchange mechanism.[15a,28b] Thus, the $\Delta E_{ST}(CT)$ values of these ICT molecules are expected to be related to $\cos\theta$ and $\cos\theta_1 \cos\theta_2$ for **a**-type and **b**-type molecules, respectively. In fact, a proportional relationship was found between $\Delta E_{ST}(CT)$ and $\cos^2\theta$ or $\cos^2\theta_1 \cos^2\theta_2$ on the basis of our calculation results (SI, Table S3), which is consistent with the prediction that J_{if} is weighted by S_{if}^2.[29] Owing to the increase of the dihedral angle θ, the ΔE_{ST} values for **a1**−**3** in the S_1 state are significantly smaller than those in the S_0 state. On the contrary, the exchange energy for **b1**−**3** in the S_1 state is slightly larger than that in the S_0 state due to the decrease of the dihedral angle θ_2.

TD-DFT also provides a relative oscillator strength (f) for each transition. Since oscillator strength of vertical absorption and emission is a function of transition energy, their optimal values were determined by a correction of those calculated at the TD-DFT/B3LYP/6-31G(d) level using

$$f_{VA}(OHF) = f_{VA}(B3LYP)E_{VA}(S_1, OHF)/E_{VA}(S_1, B3LYP) \quad (6a)$$

$$f_{VE}(OHF) = f_{VE}(B3LYP)E_{VE}(S_1, OHF)/E_{VE}(S_1, B3LYP) \quad (6b)$$

Taking a simplified relationship that allows the transition rate (s^{-1}) to be approximated by the product of the oscillator strength and the square of the wavenumber (cm^{-1}) (page 196 in ref 11), the transition rates of vertical absorption and emission can be calculated by

$$k_{VA} = f_{VA}(OHF)E_{VA}(S_1, OHF)^2 \quad (7a)$$

$$k_{VE} = f_{VE}(OHF)E_{VE}(S_1, OHF)^2 \quad (7b)$$

Unsurprisingly, the computed k_{VA} and k_{VE} are approximately proportional to $\cos^2\theta$ for **a**-type molecules and $\cos^2\theta_1 \cos^2\theta_2$ for **b**-type molecules (Tables 1 and S3) due to a roughly proportional dependence of k_V on the dihedral-angle-dependent H_{if}^2 in these ICT systems (eq 1). Since θ for **a4** and θ_1 for **b4** are predicted to be nearly 90° in both S_0 and S_1, their ICT transitions are theoretically forbidden with transition rates that are nearly zero. However, the transitions may actually be more permissible due to a conformational distribution including more planar geometries around the equilibrium one. For the same reason, their actual $\Delta E_{ST}(CT)$ may also be larger than the simulated values.

In S_0, the k_{VA} of each **a**-type molecule is similar to that of the **b**-type molecule with the same donor. For **b**-type molecules, the k_{VE} in broken-symmetry S_1 are nearly half of their k_{VA} in S_0 because the S_1 (HOMO → LUMO) and S_2 (HOMO−1 → LUMO) transitions share the overall f (Table S2). If so, the symmetrical design (e.g., D-A-D) will not lead to a higher k_F. For **a**-type molecules, the $f(S_1)$ in S_1 are much smaller than those in S_0 due to not only the symmetry breaking but also the internal rotation. Interestingly, it is found that the DTC-based molecule **b3** in S_0 has a small ΔE_{ST} (0.12 eV), which is comparable to those of the large twisted TADF emitters,[2c,e,8] but a large transition rate that is comparable to the DPA-based molecule **b1**, suggesting that a large k_F and a small ΔE_{ST} can be achieved in one molecule by adopting a **b**-type structure with well controlled θ_1 and θ_2.

Photophysical Properties. The synthesis of the eight compounds in Scheme 3 is described in the SI. Their absorption and emission spectra in toluene at room temperature are shown in Figure 3. The lowest-energy absorption bands (400−500 nm) can be ascribed to the ^{1}CT transitions. Their peak energies are consistent with the computed $E_{VA}(S_1)$ (Table S1). Except for the hardly emissive **a4** and yellow-emitting **b3**, the molecules emit orange-red to red light with peaks at 600−630 nm in toluene. The computed $E_{VE}(S_1)$ values for **a**-type molecules coincide with their emission peak energies, while those of **b**-type molecules are generally overestimated by 0.2 eV (Table S1). The polarizable continuum model used here may underestimate the solvation in toluene/**b**-type-molecule systems,[30] because the $E_{VA}(S_1)$ and $E_{VE}(S_1)$ calculated under vacuum are in good agreement with the experimental values in nonpolar solvent (Table S4, Figure S2b). The oscillator strength of the ^{1}CT absorption listed in Table 2 was determined experimentally from the integration of its band (page 195 in ref 11) by

$$f = 4.3 \times 10^{-9} \int \varepsilon \, d\tilde{\nu} \quad (8)$$

where ε is the molar extinction coefficient and $\tilde{\nu}$ is the wavenumber of the absorption. The f values for phenylamine, DTC, and DMAC derivatives decrease in order, while **a**- and **b**-type molecules with the same donor have similar f. Except for the DMAC derivatives having significantly higher f than the computed ones, the experimental f for the molecules are about two-thirds of the computed ones (Table 1).

dx.doi.org/10.1021/ja510144h | J. Am. Chem. Soc. 2014, 136, 18070−18081

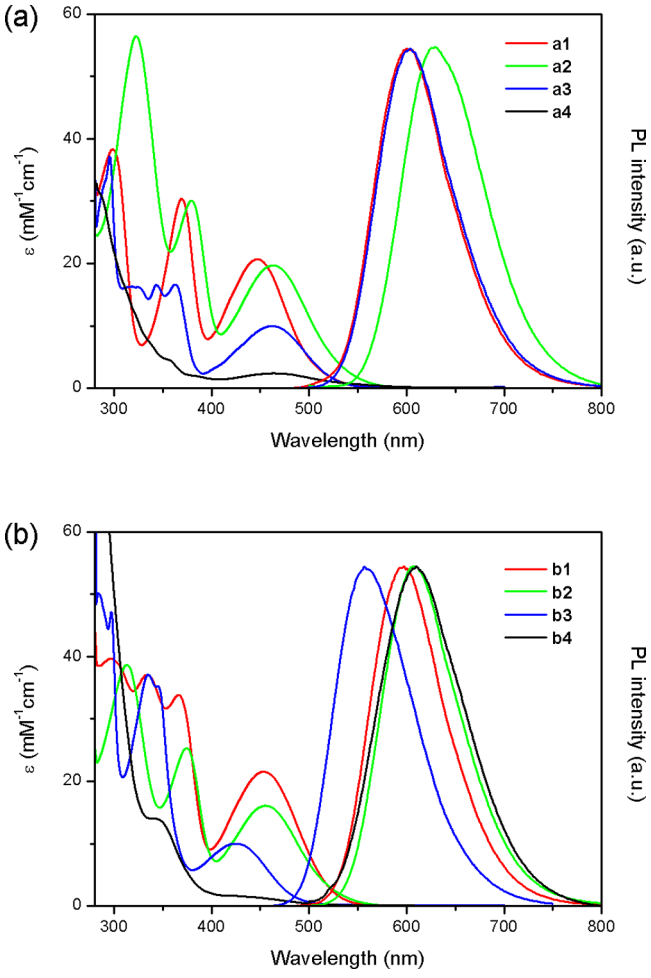

Figure 3. Absorption and emission spectra of the investigated molecules in toluene (0.02 mM) at room temperature. The low-intensity emission spectrum of **a4** is shown in Figure S2a.

According to the Strickler–Berg relationship, given little change of the molecular structure taking place in S_1, the rate constant of the emission is related to the oscillator strength of the first absorption transition by (page 196 in ref 11):

$$k_{SB} = 0.67\tilde{\nu}^2 f \quad (9)$$

where $\tilde{\nu}$ is the wavenumber of the absorption maximum of the CT band. For **b**-type molecules measured in air-saturated toluene, experimental k_F calculated by dividing Φ by the single-exponential fluorescence lifetime (τ_F) is about half of k_{SB} (Table 2). Taking into account the simulation results, we deduce that the halving of the rate constant can be attributed to the excited-state symmetry breaking, which can be further confirmed by comparing the k_{SB} and experimental k_F of an asymmetrical analogue of **b1**, DPA-Ph-AQ (SI, Figure S3). However, for **a**-type molecules **a1**–**3**, experimental k_F is significantly lower than k_{SB} (Table 2), which is in agreement with the change of transition rate between S_0 and S_1 revealed by the molecular simulations, indicating a fast relaxation by twisting in the excited state in toluene. The experimental trends of k_{SB} and k_F determined from the absorption and emission processes, respectively, match the computed trends of k_{VA} and k_{VE} but with a relationship of $k_{SB} \approx 0.5\ k_{VA}$ and $k_F \approx 0.5\ k_{VE}$ (Tables 1 and 2).

After oxygen degassing by nitrogen bubbling, Φ and τ_F of these compounds in toluene at room temperature increase significantly, accompanied by the presence of TADF with a single-exponential lifetime (τ_{TADF}) ranging from a few to hundreds of microseconds (SI, Figure S4). The relatively short τ_F in air-saturated toluene indicates that the dissolved oxygen can quench the long-lived ^{1}CT states as well as the triplet states of these molecules.[31] In oxygen-free toluene, the total Φ of **a1**–**3** are around 0.1–0.2, while those of **b1**–**3** can be as high as nearly 0.6. Due to the lack of orbital overlap, the Φ of **b4** (0.17) is dramatically lower than that of other **b**-type molecules. The fluorescence and TADF components in the transient decay spectra can be distinguished by the extension of a line fitted to the TADF decay (Figure 4), a solution to the broad instrument

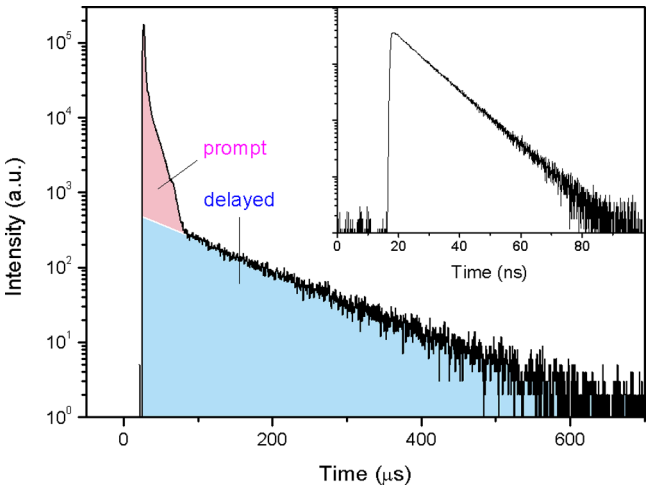

Figure 4. Transient decay spectra of **b1** in an O_2-free toluene at room temperature. The wide impulse response function (flash lamp) causes the distortion of the curve (pink) corresponding to the prompt component.

Table 2. Photophysical Data for the Investigated Molecules in Toluene at Room Temperature

	in air-saturated toluene							in O_2-free toluene				
	$\lambda_{abs,max}$ (nm)	f	$\lambda_{em,max}$ (nm)	Φ	τ_F (ns)	k_F ($\times 10^7$ s^{-1})	k_{SB} ($\times 10^7$ s^{-1})	Φ	Φ_F	τ_F (ns)	τ_{TADF} (μs)	k_F ($\times 10^7$ s^{-1})
a1	449	0.36	601	0.09	3.6	2.5	12.4	0.20	0.13	5.3	377	2.5
a2	464	0.37	629	0.06	2.6	2.3	12.0	0.10	0.08	3.5	74	2.3
a3	463	0.18	602	0.07	4.0	1.8	5.8	0.15	0.13	7.5	7.7	1.7
a4	527	0.015	662									
b1	454	0.36	597	0.30	4.9	6.1	12.2	0.59	0.55	9.0	102	6.1
b2	456	0.30	608	0.25	5.1	4.9	10.0	0.62	0.55	11.2	85	4.9
b3	426	0.19	558	0.43	9.4	4.6	7.4	0.60	0.58	12.6	17.0	4.6
b4	446	0.018	609	0.02	6.7	0.30	0.63	0.17	0.13	42	3.5	0.31

dx.doi.org/10.1021/ja510144h | J. Am. Chem. Soc. 2014, 136, 18070–18081

Table 3. Photophysical Data for the Investigated Molecules Doped into CBP Films (1 wt%) at Room Temperature

	$\lambda_{em,max}$ (nm)	Φ	Φ_F	τ_F (ns)	τ_{TADF} (μs)	k_F ($\times 10^7$ s^{-1})	k_{IC} ($\times 10^7$ s^{-1})	k_{ISC} ($\times 10^7$ s^{-1})	k_{TADF} ($\times 10^4$ s^{-1})	ΔE_{ST} (eV)
a1	593	0.50	0.13	4.9	4600[a]	2.7	2.6	15	0.011	0.29
a2	603	0.42	0.17	5.6	1560[a]	3.0	4.2	11	0.027	0.27
a3	575	0.52	0.16	10.4	62[a]	1.5	1.4	6.5	0.84	0.17
a4	600	0.08	0.05	16.5[a]	1.6	0.30	3.5	2.3	5.1	0.08
b1	594	0.80	0.54	10.2	416[a]	5.3	1.3	3.2	0.19	0.24
b2	601	0.76	0.54	10.2	185[a]	5.3	1.7	2.8	0.41	0.22
b3	550	0.65	0.12	33[a]	16/156	0.36	0.19	2.4		
b4	564	0.50	0.14	41[a]	6.5[a]	0.34	0.34	1.7	7.7	0.07

[a]An average lifetime calculated by $\tau_{av} = \sum A_i\tau_i^2/\sum A_i\tau_i$, where A_i is the pre-exponential for lifetime τ_i (A_i and τ_i are shown in SI, Figure S7).

response for the fluorescence decay. The fluorescent (Φ_F) and TADF (Φ_{TADF}) components of Φ are subsequently determined from the total Φ and the proportion of the integrated area of each of the components in the transient spectra to the total integrated area. The k_F values calculated from Φ_F and τ_F in oxygen-free toluene are found to be equal to those in air-saturated solutions (Table 2).

With the goal of application in devices, the photophysical properties of the title compounds were investigated by doping them into 4,4′-bis(carbazol-9-yl)biphenyl (CBP), which is the most commonly used host material for green and red phosphors and has a high $E_{0-0}(T_1)$ of 2.6 eV (Table 3). To lower aggregation induced red-shifting and quenching (see SI, Figure S5) so as to better compare the data in solution and films, a low doping concentration of 1 wt% was adopted in the following PL studies. In comparison with the emission spectra in toluene, those in 1wt%-doped CBP films are blue-shifted by 2−62 nm (SI, Figure S6, Tables 2 and 3) because the highly polar ^{1}CT states cannot be stabilized by the reorganization of surrounding polar molecules when doped in a solid matrix. Except for **b3**, the fluorescence and TADF decay for these molecules in doped films can be well fitted by a single or a double exponentials (Figures 5a and S7), and the individual Φ_F and Φ_{TADF} can be calculated in the same way as in toluene. Weighted average fluorescence lifetimes (Table 3) were used to calculate k_F for the molecules with double exponential fluorescence decay. For the molecules other than **b3**, their k_F in CBP film are close to those in toluene (Table 2), implying that **a**-type molecules can undergo a 10−20° rotational excited state relaxation even in organic semiconductor films. However, the excited-state conformation distribution of **a**-type molecules with large donor units should be wide due to their heterogeneous microenvironment in the solid films. Not surprisingly, the streak image (300 K) of an **a2**-doped film reveals a blue-shifted emission band based on its long-lived TADF component (>2.5 ms) (Figure 5a insert). The component may arise from rotamers that are more planar and whose rotational relaxations are restricted by their rigid microenvironment.

The photophysical properties of **b3** in doped CBP films are special among these molecules. Its fluorescence decay is double exponential while its TADF decay is a multi-exponential that can be roughly divided into two components (Figure 5b). The fast component (68%) of TADF has a single-exponential decay time of 16 μs, while the slow one (32%) has a single-exponential decay time of 156 μs. The two TADF components appear to arise from two different rotamers in the doped film because of the different spectra observed for these two components from streak images (Figure 5b insert). Since the k_F value of **b3** (3.3×10^6 s^{-1}) in the doped film is significantly

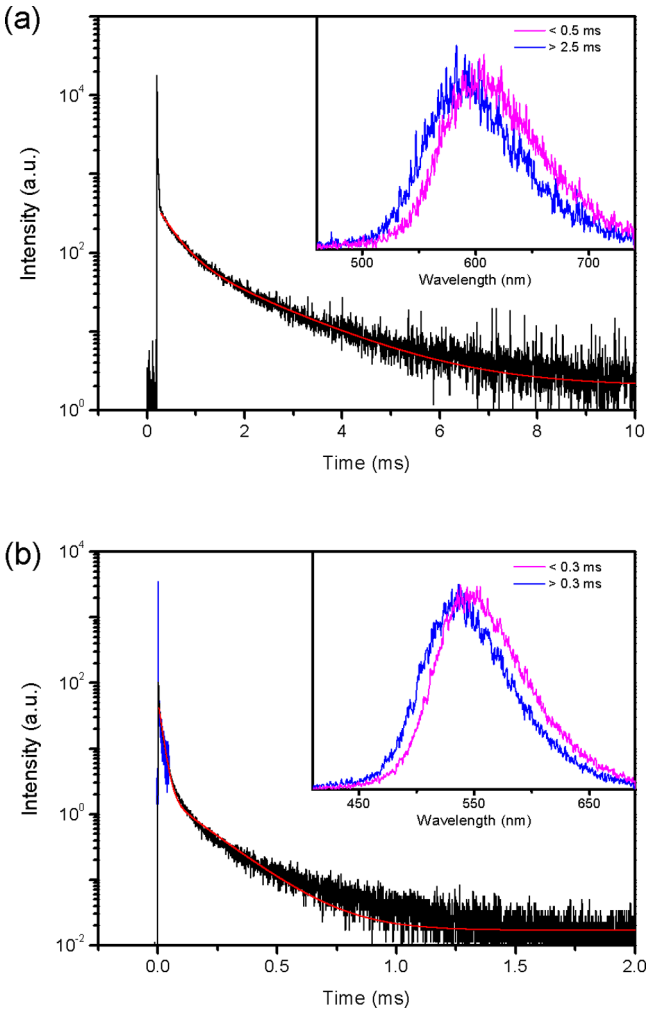

Figure 5. Transient decay spectra of (a) **a2** and (b) **b3** doped into CBP films (1 wt%) measured with a fluorescence lifetime spectrometer (C11367-03, Hamamatsu Photonics) at room temperature. Black curves were recorded in TCC900 mode; blue curves were recorded in M9003-01 mode; red curves are double-exponential fitting data. Inset: Emission spectra of TADF components measured by a streak camera at room temperature.

smaller than that in toluene (4.6×10^7 s^{-1}), the predominant rotamer in the doped film should be more tortile than the one in toluene. The formation of differently twisted **b3** can be explained with Scheme 4. In the doped film, about three-fourths of **b3** molecules in S_0 contain at least one D-π-A moiety twisted like model I (I-I, I-II, II-I), while one-fourth of them are only twisted like model II (II-II). For the former, the flattening distortion of the Ph-bridge with respect to AQ-acceptor in S_1

dx.doi.org/10.1021/ja510144h | J. Am. Chem. Soc. 2014, 136, 18070−18081

may enlarge the dihedral angle θ_1 between the Ph-bridge and the rotationally restricted DTC-donor, resulting in a decrease of k_F, ΔE_{ST}, and τ_{TADF}. In contrast, the species containing only model II twisting tend to relax toward a more planar conformation in S_1 with increased k_F, ΔE_{ST}, and τ_{TADF}.

Since TADF emitters in rigid matrices cannot undergo deactivation through collisions with surrounding molecules (page 288 in ref 11), their Φ in doped CBP films are considerably higher than those in solution (Tables 2 and 3). Even **a4**, which showed almost no emission in toluene, has a Φ of 0.08 in the doped film. According to the Boltzmann distribution, the time the title molecules spend in T_1 is much longer than that in S_1 when S_1 and T_1 achieve thermal equilibrium, so the collision-free condition favors the suppression of non-radiative decay from T_1 to S_0. This is consistent with the fact that the Φ_F and τ_F in doped films are comparable with the corresponding values in oxygen-free toluene while the Φ_{TADF} and τ_{TADF} in the former are much higher than those in the latter (Tables 2 and 3). In particular, **a1** and **a2** show extremely long TADF lifetimes of 4.6 and 1.6 ms in the doped films (Figure S7). Since the IC process is generally 4−8 orders of magnitude faster than ISC with a similar band gap,[32] it seems reasonable to assume that the IC process from S_1 to S_0 dominates the deactivation of the TADF emitters in the doped films;[33] therefore, the k_{IC}, k_{ISC}, and k_{TADF} can be given by the following formulas:

$$\Phi = k_F/(k_F + k_{IC}) \quad (10)$$

$$\Phi_F = k_F/(k_F + k_{IC} + k_{ISC}) \quad (11)$$

$$\Phi_{IC} = k_{IC}/(k_F + k_{IC} + k_{ISC}) \quad (12)$$

$$\Phi_{ISC} = 1 - \Phi_F - \Phi_{IC} = k_{ISC}/(k_F + k_{IC} + k_{ISC}) \quad (13)$$

$$k_{TADF} = \Phi_{TADF}/\Phi_{ISC}\tau_{TADF} \quad (14)$$

where Φ_{ISC} is the triplet yield ignoring the reverse ISC from T_1 to S_1. Note that k_{TADF} approximates Φ_{TADF}/τ_{TADF} only in the case of $k_{ISC} \gg k_{IC} + k_F$.[2e] As shown in Figure 6, the k_{IC} in doped CBP films seems to be governed by the D-A distance as well as the energy gap law (i.e., $\ln(k_{IC}) \propto E_{VE}(S_1)^{-1}$). For the same $E_{VE}(S_1)$, the k_{IC} of an **a**-type molecule is more than twice as high as that of a **b**-type molecule, owing to the so-called free rotor and loose bolt effects in **a**-type molecules (page 288 in ref 11). As predicted by TD-DFT, the S_1 of **a**-type molecules can be stabilized by twisting and stretching of the N−C bond between a donor and acceptor, which shows some π-bond character when the twisting angle θ is smaller than 90°. According to radiationless transition theory, twisting a π bond or stretching a σ bond in S_1 causes an approaching of surfaces that facilitates IC to S_0 (Scheme 5). The numerous

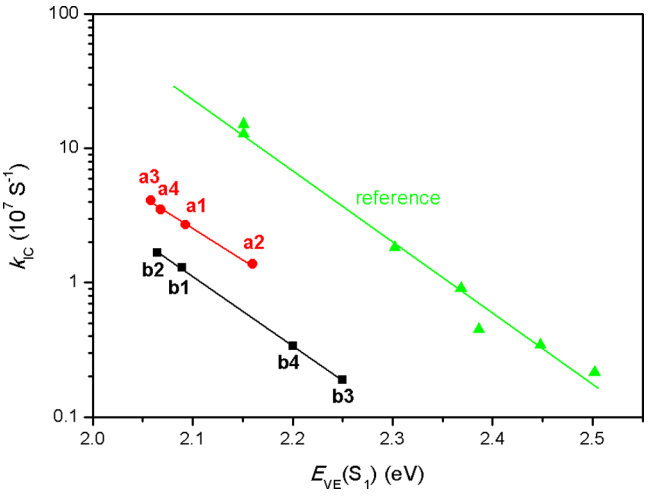

Figure 6. Plot of the rate constants of internal conversion between S_1 and S_0 (k_{IC}) versus vertical emission energy (E_{VE}) for the investigated molecules doped into CBP films (1 wt%) at room temperature. The reference data are from reported TADF emitters based on a diphenylsulfone acceptor in various solvents (Supporting Information in ref 2e).

Scheme 5. Stretching of a σ Bond or Twisting of a π Bond Lowers the Energy of ^{1}CT State (S_1) but Raises the Energy of the Ground State (S_0), Resulting in the S_1 and S_0 Surfaces Approaching Each Other and Creating a More Efficient Radiationless Deactivation Pathway (Energy Gap Law)

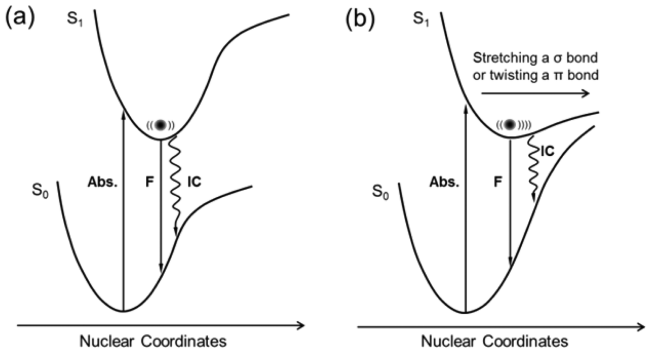

investigations on MLCT Cu(I) complexes also indicated that a rigid conformation is crucial to suppress radiationless relaxation of the exciplex back to ground state and improve its Φ.[14] Since the free rotor and loose bolt effects can also operate to facilitate the ISC process, the values of k_{ISC} for **a**-type molecules are also found to be higher than those for **b**-type molecules (Table 3).

Due to the low phosphorescence yield of the title molecules in toluene and doped films at low temperatures (SI, Figure S8), it is hard to reliably estimate ΔE_{ST} from their fluorescence and phosphorescence spectra. In addition, solvent glasses can restrict the rotational relaxation of these molecules in the excited state, and therefore ΔE_{ST} values obtained in them do not represent the ones at room temperature. Here, we calculated the ΔE_{ST} of these molecules in doped films at room temperature by using an approximate relationship among ΔE_{ST}, k_{TADF}, and k_F as follows:[2e]

$$k_{TADF} = (1/3)[k_F \exp(-\Delta E_{ST}/RT)] \quad (15)$$

where R and T denote the ideal gas constant and absolute temperature, respectively. Equation 15 is simplified from a more general expression for the temperature dependence of the lifetime of two thermally equilibrated emitting states when the gap between these two states is in the range of 0.05−0.30 eV.[2e,5b] The ΔE_{ST} values of these molecules in doped films given by eq 15 are close to the values computed on the basis of their S_1 geometries (Tables 1 and 3). On the other hand, the experimental ΔE_{ST} values of **a1**−**3** are significantly lower than the corresponding values simulated in the S_0 geometries, suggesting that intramolecular twisting relaxations occur in doped films after excitation. Since ΔE_{ST} is insensitive to k_{TADF}

dx.doi.org/10.1021/ja510144h | J. Am. Chem. Soc. 2014, 136, 18070−18081

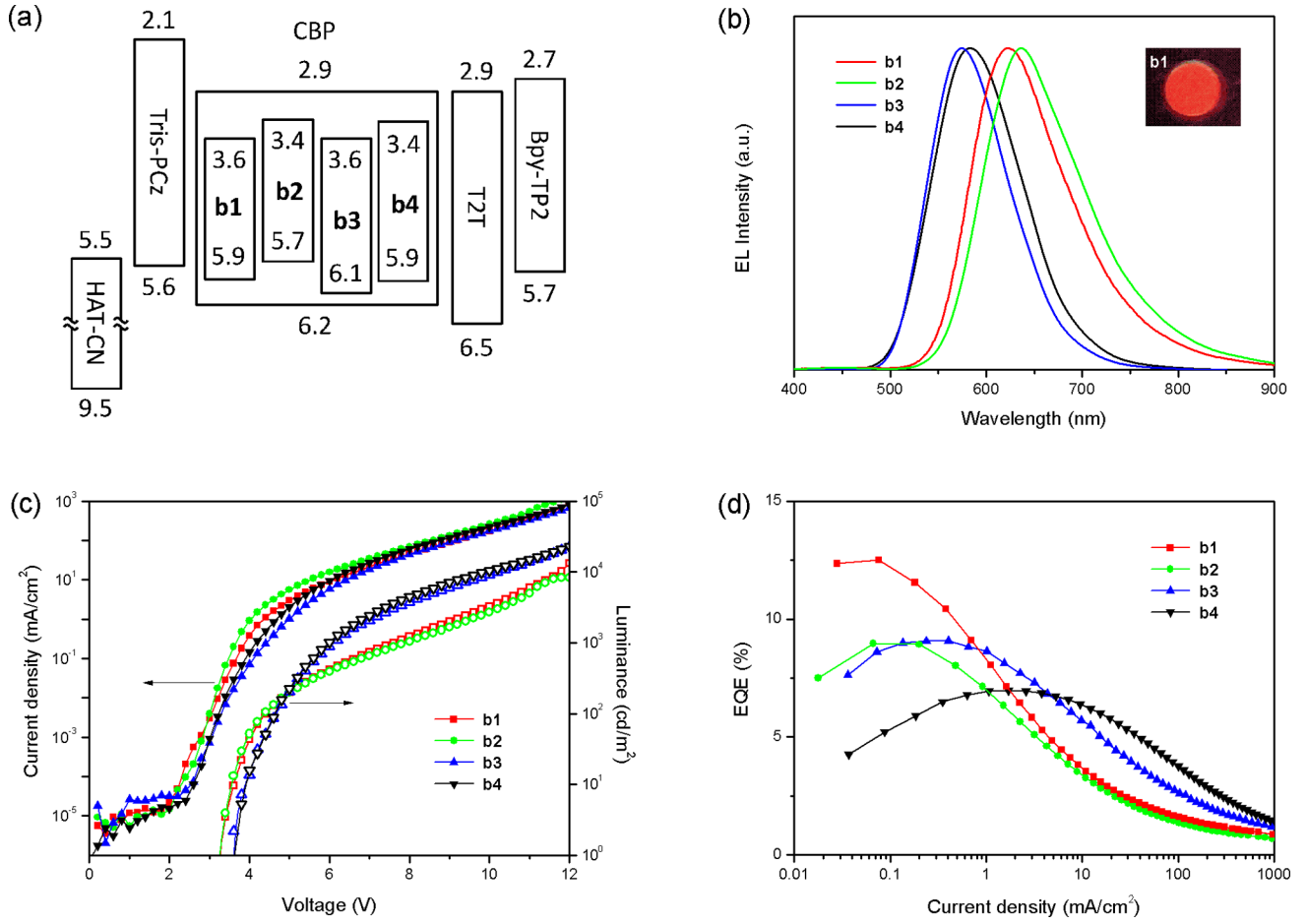

Figure 7. (a) Energy diagram of OLEDs. HOMO levels of CBP and **b1**−**4** were measured by photoelectron spectroscopy (AC-3). Their energy gaps were determined from the absorption edge, and their LUMO levels were calculated from the HOMO minus the energy gap. HOMO and LUMO levels of other materials are taken from literature values.[34] (b) EL spectra at 10 mA/cm^2 (inset: image of **b1**-based OLED), (c) luminance−current density−voltage characteristics, and (d) EQE−current density characteristics of the OLEDs based on **b1**−**4**.

(e.g., ΔE_{ST} decreases only 0.01 eV when k_{TADF} doubles), we can also estimate the ΔE_{ST} of some efficient emitters ($k_F > k_{IC}$) in solution using eqs 14 and 15 with an approximation of $\Phi_{ISC} \approx 1 - \Phi_F$. The reliability of such a treatment has been confirmed by using reported TADF emitters with ΔE_{ST} determined in toluene (SI, Table S5).

Device Characterization. From the previous comparison, we can conclude that the **b**-type molecules are more suitable for application in OLEDs owing to their relatively high Φ and short τ_{TADF} in doped films. Consequently, the four **b**-type molecules were selected for characterization in devices with an optimized structure (SI, Figure S9),[34] indium tin oxide (ITO)/HAT-CN (10 nm)/Tris-PCz (30 nm)/10 wt% TADF:CBP (30 nm)/T2T (10 nm)/Bpy-TP2 (40 nm)/LiF (0.8 nm)/Al, where dipyrazino[2,3-*f*:20,30-*h*]quinoxaline-2,3,6,7,10,11-hexacarbonitrile (HAT-CN), 9,9′-diphenyl-6-(9-phenyl-9*H*-carbazol-3-yl)-9*H*,9′*H*-3,3′-bicarbazole (Tris-PCz), 2,4,6-tris(biphenyl-3-yl)-1,3,5-triazine (T2T), 2,7-bis(2,20-bipyridin-5-yl)-triphenylene (Bpy-TP2), and LiF act as hole injection, hole transport, exciton-blocking, electron transport, and electron injection layers, respectively. An energy diagram of the devices is shown in Figure 7a. The HOMO and LUMO levels of **b1**−**4** are above and below those of the CBP host, suggesting that hole−electron capture by these emitters in the emitting layers (EMLs) can be balanced. To achieve a complete Dexter energy transfer from the CBP host to the TADF emitters, a relatively high doping concentration of 10 wt% was adopted for these TADF OLEDs (the doping-concentration-dependent PL and EL performance of **b1** in a CBP host can be found in Figures S5 and S10). However, similar to most ICT molecules, these TADF emitters also suffered from aggregation-induced quenching to some degree, accompanied by an emission red-shift. The emission maxima and Φ of **b1**−**4** in 10 wt% doped CBP films are 613 nm and 0.55, 626 nm and 0.40, 565 nm and 0.41, and 570 nm and 0.32, respectively.

The EL spectra of these OLEDs are shown in Figure 7b. They have a small red-shift (∼10 nm) with respect to the PL spectra of the EMLs. The **b1**- and **b2**-based OLEDs emit red light with emission peaks at 624 and 637 nm and Commission Internationale de L'Eclairage (CIE) coordinates of (0.61, 0.39) and (0.63, 0.37), respectively. On the other hand, the **b3**- and **b4**-based OLEDs emit orange light with emission peaks at 574 and 584 nm, respectively. As shown in Figure 7c, these four devices turn-on at 3 V and achieved maxima luminance of 10 000−30 000 cd/m^2 at about 12 V. As shown in Figure 7d, the maxima external EL quantum efficiencies (EQEs) of the devices based on **b1**−**4** are 12.5%, 9.0%, 9.0%, and 6.9%, respectively. On the basis of the investigations of the PL properties in doped films (see also ref 33), we can conclude that $S_1 \rightarrow S_0$ IC is the major radiationless deactivation pathway for these TADF emitters in OLEDs with low doping concentrations at low current density. As a consequence, the

dx.doi.org/10.1021/ja510144h | J. Am. Chem. Soc. 2014, 136, 18070−18081

triplet TADF emitters will have the same quantum yields as the singlet ones, and the maximum IQEs of the devices will be close to the total Φ of the TADF dopants in EMLs even though three-fourths of excitons generated by hole−electron recombination in OLEDs are in the T_1 state. Although the complicated bimolecular quenching processes cannot be ignored at higher doping concentrations like 10 wt%, the maximum IQEs of these TADF OLEDs are close to the Φ of their EMLs when a light out-coupling efficiency of 0.2−0.3 is assumed.

Although the EQEs of the red TADF OLEDs containing **b1** and **b2** at low current density are comparable with those of the devices containing tris[1-phenylisoquinolinato-C2,N]iridium-(III) ($Ir(piq)_3$),[3c] a classical red phosphorescent material, their efficiencies at high current densities are lower than those of the $Ir(piq)_3$-based OLED (SI, Figure S11). The EQEs of **b1**- and **b2**-based OLEDs decrease to 8.1% and 5.7% at a luminance of 100 cd/m^2 and to 2.3% and 1.7% at a luminance of 1000 cd/m^2, respectively. The fast EQE roll-off with increasing current density can be attributed to the long TADF lifetimes of **b1** and **b2** in doped films, which are 2 orders of magnitude higher than that of $Ir(piq)_3$.[3c] As revealed by numerous previous studies, long-lived triplet excitons are more easily be quenched by TTA, STA, and TPA processes, which are highly dependent on the current density in the device.[10] Although the EQE roll-off of the **b1**- and **b2**-based OLEDs is not observably improved over that of reported orange-red TADF OLEDs (λ_{max} = 610 nm) based on a diphenylamine/heptazine derivative (HAP-3TPA),[2d] the ΔE_{ST} have been successfully reduced from 0.30 eV for HAP-3TPA (by OHF/TD-DFT) to 0.21 eV for **b2** without significantly lowering the Φ in doped films. Since **b4** in CBP has a short TADF lifetime on the order of microseconds, the EQE roll-off is significantly reduced in its device with an EQE at 1000 cd/m^2 of 94% of the maximum. In doped CBP films, a fraction of the **b3** rotamers have a short TADF lifetime comparable with that of **b4** while others have a long TADF lifetime comparable with that of **b2**. As a result, the degree of efficiency roll-off for **b3**-based OLEDs is between those of **b2**- and **b4**-based OLEDs. Despite good performance at high current density, it is worth noting that the **b4**-based OLED emits orange light. If the highly twisted ICT molecules have redder emission, their Φ will dramatically decrease because their low k_F values cannot compete with the quickly growing k_{IC}, just as in the case of **b4** in toluene. Finding a balance between k_F and ΔE_{ST} by adjusting the twisting angles in new **b**-type molecules is our next step but also a challenge.

CONCLUSIONS

Increasing the transition rate without enlarging the overlap of the involved orbitals is a key in the realization of efficient red TADF emitters having fast TADF. Herein, we approached this goal by enlarging the effective separation distance of appropriate donors and an acceptor to increase the dipole-moment change in the CT transition. The comparison of eight TADF emitters with DPA, BBPA, DTC, and DMAC donors and an AQ acceptor indicates that D-Ph-A (**b**)-type TADF emitters have higher k_F and consequently higher Φ relative to D-A (**a**)-type TADF emitters with the same ΔE_{ST}. In addition, it was found that the N−C bond linking the donor and acceptor in D-A-type emitters twists and stretches in S_1 to stablize the excited state, leading to smaller ΔE_{ST}, lower k_F, and more efficient radiationless $S_1 \rightarrow S_0$ IC and $S_1 \rightarrow T_1$ ISC processes. The rotational excited-state relaxation was found to occur even in organic semiconductor films. Since most D-Ph-A-type emitters show only minor geometry rearrangement in the excited state, they have smaller k_{IC} compared to the D-A-type emitters with the same emission energy, which further contributes to their higher Φ. A D-Ph-A-type emitter based on DPA as donor (**b1**) exhibits a high Φ of 0.55 with an emission peak at 614 nm and a relatively short TADF lifetime of 120 μs in 10 wt%-doped CBP film. The OLED using this doped film as EML achieved an EQE up to 8.1% at a luminance of 100 cd/m^2 with an emission maximum at 624 nm, which are comparable to the values for the best red PHOLEDs.

It is noteworthy that the quantum yield of red TADF emitters can be further improved by selecting a new π-bridge with longer axial length and donors and acceptors with larger atomic orbital coefficients. Molecular design will be facilitated by using an optimal HF exchange method based on TD-DFT, which has effectively reproduced various photophysical parameters of studied TADF molecules. The molecule simulation in this work suggested that a fast transition rate and a small ΔE_{ST} can be achieved in one molecule by well controlling the twisting angles of a **b**-type molecule. However, the design idea may be partially unfulfilled due to the flattening of the Ph-bridge and acceptor and a subsequent twisting of the Ph-bridge and donor in doped films. Therefore, suppressing undesirable rotational relaxation in the excited state is as important as controlling the twisting angles between the subunits in S_0. In addition, suppressing rotational relaxation generally results in a narrower emission band, allowing the realization of purer red colors without lowering the energy gap.

ASSOCIATED CONTENT

Supporting Information

Supplemental tables and figures; experimental details; synthesis and computational geometries of the investigated compounds. This material is available free of charge via the Internet at http://pubs.acs.org.

AUTHOR INFORMATION

Corresponding Author

adachi@cstf.kyushu-u.ac.jp

Author Contributions

[§]Q.Z. and H.K. contributed equally.

Notes

The authors declare no competing financial interest.

ACKNOWLEDGMENTS

This work was supported by the Funding Program for World-Leading Innovative R&D on Science and Technology (FIRST) and the Exploratory Research for Advanced Technology (ERATO). The authors thank Prof. Katsumi Tokumaru and Dr. Katsuyuki Shizu for stimulating discussions with regard to this work.

REFERENCES

(1) (a) Boudin, M. S. *J. Chim. Phys.* **1930**, *27*, 285. (b) Saltiel, J.; Curtis, H. C.; Metts, L.; Miley, J. W.; Winterle, J.; Wrighton, M. *J. Am. Chem. Soc.* **1970**, *92*, 410. (c) Herbich, J.; Kapturkiewicz, A.; Nowacki, J. *Chem. Phys. Lett.* **1996**, *262*, 633. (d) Heinz, B.; Schmidt, B.; Root, C.; Satzger, H.; Milota, F.; Fierz, B.; Kiefhaber, T.; Zintha, W.; Gilch, P. *Phys. Chem. Chem. Phys.* **2006**, *8*, 3432. (e) Baleizao, C.; Berberan-Santos, M. N. *Ann. N.Y. Acad. Sci.* **2008**, *1130*, 224.

(2) (a) Endo, A.; Sato, K.; Yoshimura, K.; Kai, T.; Kawada, A.; Miyazaki, H.; Adachi, C. *Appl. Phys. Lett.* **2011**, *98*, No. 083302. (b) Zhang, Q.; Li, J.; Shizu, K.; Huang, S.; Hirata, S.; Miyazaki, H.;

Adachi, C. *J. Am. Chem. Soc.* **2012**, *134*, 14706. (c) Uoyama, H.; Goushi, K.; Shizu, K.; Nomura, H.; Adachi, C. *Nature* **2012**, *492*, 234. (d) Li, J.; Nakagawa, T.; MacDonald, J.; Zhang, Q.; Nomura, H.; Miyazaki, H.; Adachi, C. *Adv. Mater.* **2013**, *25*, 3319. (e) Zhang, Q.; Li, B.; Huang, S.; Nomura, H.; Tanaka, H.; Adachi, C. *Nat. Photonics* **2014**, *8*, 326.

(3) (a) Ma, Y.; Zhang, H.; Shen, J.; Che, C. *Synth. Met.* **1998**, *94*, 245. (b) Baldo, M. A.; O'Brien, D. F.; You, Y.; Shoustikov, A.; Sibley, S.; Thompson, M. E.; Forrest, S. R. *Nature* **1998**, *395*, 151. (c) Tsuboyama, A.; Iwawaki, H.; Furugori, M.; Mukaide, T.; Kamatani, J.; Igawa, S.; Moriyama, T.; Miura, S.; Takiguchi, T.; Okada, S.; Hoshino, M.; Ueno, K. *J. Am. Chem. Soc.* **2003**, *125*, 12971. (d) Chou, P.-T.; Chi, Y. *Eur. J. Inorg. Chem.* **2006**, 3319. (e) Yook, K. S.; Lee, J. Y. *Adv. Mater.* **2012**, *24*, 3169. (f) Sasabe, H.; Kido, J. *J. Mater. Chem. C* **2013**, *1*, 1699.

(4) (a) Zhang, Q.; Zhou, Q.; Cheng, Y.; Wang, L.; Ma, D.; Jing, X.; Wang, F. *Adv. Funct. Mater.* **2006**, *16*, 1203. (b) Deaton, J. C.; Switatski, S. C.; Kondakov, D. Y.; Young, R. H.; Pawlik, T. D.; Giesen, D. J.; Harkins, S. B.; Miller, A. J. M.; Mickenberg, S. F.; Peters, J. C. *J. Am. Chem. Soc.* **2010**, *132*, 9499. (c) Hashimoto, M.; Igawa, S.; Yashima, M.; Kawata, I.; Hoshino, M.; Osawa, M. *J. Am. Chem. Soc.* **2011**, *133*, 10348. (d) Hsu, C.-W.; Lin, C.-C.; Chung, M.-W.; Chi, Y.; Lee, G.-H.; Chou, P.-T.; Chang, C.-H.; Chen, P.-Y. *J. Am. Chem. Soc.* **2011**, *133*, 12085. (e) Zhang, Q.; Komino, T.; Huang, S.; Matsunami, S.; Goushi, K.; Adachi, C. *Adv. Funct. Mater.* **2012**, *22*, 2327. (f) Liu, Z.; Qiu, J.; Wei, F.; Wang, J.; Liu, X.; Helander, M. G.; Rodney, S.; Wang, Z.; Bian, Z.; Lu, Z.; Thompson, M. E.; Huang, C. *Chem. Mater.* **2014**, *26*, 2368.

(5) (a) Blasse, G.; McMillin, D. R. *Chem. Phys. Lett.* **1980**, *70*, 1. (b) Kirchhoff, J. R.; Gamache, R. E.; Blaskie, M. W.; Del Paggio, A. A.; Lengel, R. L.; McMillin, D. R. *Inorg. Chem.* **1983**, *22*, 2380. (c) Tsuboyama, A.; Kuge, K.; Furugori, M.; Okada, S.; Hoshino, M.; Ueno, K. *Inorg. Chem.* **2007**, *46*, 1992. (d) Czerwieniec, R.; Yu, J.; Yersin, H. *Inorg. Chem.* **2011**, *50*, 8293.

(6) (a) Goushi, K.; Yoshida, K.; Sato, K.; Adachi, C. *Nat. Photonics* **2012**, *6*, 253. (b) Goushi, K.; Adachi, C. *Appl. Phys. Lett.* **2012**, *101*, No. 023306. (c) Graves, D.; Jankus, V.; Dias, F. B.; Monkman, A. *Adv. Funct. Mater.* **2014**, *24*, 2343. (d) Hung, W.-Y.; Fang, G.-C.; Lin, S.-W.; Cheng, S.-H.; Wong, K.-T.; Kuo, T.-Y.; Chou, P.-T. *Sci. Rep.* **2014**, *4*, 5161.

(7) (a) Nakagawa, T.; Ku, S.-Y.; Wong, K.-T.; Adachi, C. *Chem. Commun.* **2012**, *48*, 9580. (b) Mehes, G.; Nomura, H.; Zhang, Q.; Nakagawa, T.; Adachi, C. *Angew. Chem., Int. Ed.* **2012**, *51*, 11311. (c) Nasu, K.; Nakagawa, T.; Nomura, H.; Lin, C.-J.; Cheng, C.-H.; Tseng, M.-R.; Yasuda, T.; Adachi, C. *Chem. Commun.* **2013**, *49*, 10385.

(8) (a) Tanaka, H.; Shizu, K.; Miyazaki, H.; Adachi, C. *Chem. Commun.* **2012**, *48*, 11392. (b) Tanaka, H.; Shizu, K.; Nakanotani, H.; Adachi, C. *Chem. Mater.* **2013**, *25*, 3766. (c) Lee, S. Y.; Yasuda, T.; Yang, Y. S.; Zhang, Q.; Adachi, C. *Angew. Chem., Int. Ed.* **2014**, *53*, 6402.

(9) (a) Komino, T.; Tanaka, H.; Adachi, C. *Chem. Mater.* **2014**, *26*, 3665. (b) Mayr, C.; Lee, S. Y.; Schmidt, T. D.; Yasuda, T.; Adachi, C.; Brütting, W. *Adv. Funct. Mater.* **2014**, *24*, 5232. (c) Sun, J. W.; Lee, J.-H.; Moon, C.-K.; Kim, K.-H.; Shin, H.; Kim, J.-J. *Adv. Mater.* **2014**, *26*, 5684. (d) Nakanotani, H.; Higuchi, T.; Furukawa, T.; Masui, K.; Morimoto, K.; Numata, M.; Tanaka, H.; Sagara, Y.; Yasuda, T.; Adachi, C. *Nat. Commun.* **2014**, *5*, 4016. (e) Zhang, D.; Duan, L.; Li, C.; Li, Y.; Li, H.; Zhang, D.; Qiu, Y. *Adv. Mater.* **2014**, *26*, 5050. (f) Nishide, J.-i.; Nakanotani, H.; Hiraga, Y.; Adachi, C. *Appl. Phys. Lett.* **2014**, *104*, No. 233304. (g) Ishimatsu, R.; Matsunami, S.; Kasahara, T.; Mizuno, J.; Edura, T.; Adachi, C.; Nakano, K.; Imato, T. *Angew. Chem., Int. Ed.* **2014**, *53*, 6993.

(10) (a) Baldo, M. A.; Adachi, C.; Forrest, S. R. *Phys. Rev. B* **2000**, *62*, 10967. (b) Song, D.; Zhao, S.; Luo, Y.; Aziz, H. *Appl. Phys. Lett.* **2010**, *97*, No. 243304. (c) Masui, K.; Nakanotani, H.; Adachi, C. *Org. Electron.* **2013**, *14*, 2721.

(11) Turro, N. J.; Ramamurthy, V.; Scaiano, J. C. *Modern Molecular Photochemistry of Organic Molecules*; University Science Books: Sausalito, CA, 2010.

(12) (a) Grabowski, Z. R.; Rotkiewicz, K. *Chem. Rev.* **2003**, *103*, 3899. (b) Kapturkiewicz, A.; Herbich, J.; Nowacki, J. *Chem. Phys. Lett.* **1997**, *275*, 355.

(13) (a) Newton, M. D. *Chem. Rev.* **1991**, *91*, 767. (b) Barbara, P. F.; Meyer, T. J.; Ratner, M. A. *J. Phys. Chem.* **1996**, *100*, 13148.

(14) (a) Miller, M. T.; Gantzel, P. K.; Karpishin, T. B. *J. Am. Chem. Soc.* **1999**, *121*, 4292. (b) Scaltrito, D. V.; Thompson, D. W.; O'Callaghan, J. A.; Meyer, G. J. *Coord. Chem. Rev.* **2000**, *208*, 243. (c) Felder, D.; Nierengarten, J.-F.; Barigelletti, F.; Ventura, B.; Armaroli, N. *J. Am. Chem. Soc.* **2001**, *123*, 6291. (d) Yam, V. W.-W.; Cheng, E. C.-C.; Zhu, N. *Chem. Commun.* **2001**, *37*, 1028. (e) Riesgo, E. C.; Hu, Y.-Z.; Bouvier, F.; Thummel, R. P.; Scaltrito, D. V.; Meyer, G. J. *Inorg. Chem.* **2001**, *40*, 3413. (f) Zhang, Q.; Cheng, Y.; Wang, L.; Xie, Z.; Jing, X.; Wang, F. *Adv. Funct. Mater.* **2007**, *17*, 2983. (g) Zink, D. M.; Bächle, M.; Baumann, T.; Nieger, M.; Kühn, M.; Wang, C.; Klopper, W.; Monkowius, U.; Hofbeck, T.; Yersin, H.; Bräse, S. *Inorg. Chem.* **2013**, *52*, 2292. (h) Krylova, V. A.; Djurovich, P. I.; Conley, B. L.; Haiges, R.; Whited, M. T.; Williams, T. J.; Thompson, M. E. *Chem. Commun.* **2014**, *50*, 7176.

(15) (a) Plate, M.; Mobius, K.; Michel-Beyerle, M. E.; Bixon, M.; Jortner, J. *J. Am. Chem. Soc.* **1988**, *110*, 7279. (b) Troisi, A.; Orlandi, G. *J. Phys. Chem. B* **2002**, *106*, 2093.

(16) Itoh, T. *Chem. Rev.* **1995**, *95*, 2351.

(17) (a) Runge, E. E.; Gross, K. U. *Phys. Rev. Lett.* **1984**, *52*, 997. (b) Marques, M. A. L.; Gross, E. K. U. *Annu. Rev. Phys. Chem.* **2004**, *55*, 427.

(18) (a) Magyar, R. J.; Tretiak, S. *J. Chem. Theory Comput.* **2007**, *3*, 976. (b) Harbach, P. H. P.; Dreuw, A. The Art of Choosing the Right Quantum Chemical Excited-State Method for Large Molecular Systems. In *Modeling of Molecular Properties*; Comba, P., Ed.; Wiley-VCH: Weinheim, 2011; pp 37−38. (c) Guido, C. A.; Knecht, S.; Kongsted, J.; Mennucci, B. *J. Chem. Theory Comput.* **2013**, *9*, 2209.

(19) (a) Dreuw, A.; Head-Gordon, M. *Chem. Rev.* **2005**, *105*, 4009. (b) Peach, M. J. G.; Benfield, P.; Helgaker, T.; Tozer, D. J. *J. Chem. Phys.* **2008**, *128*, No. 044118. (c) Jacquemin, D.; Perpète, E. A.; Ciofini, I.; Adamo, C.; Valero, R.; Zhao, Y.; Truhlar, D. G. *J. Chem. Theory Comput.* **2010**, *6*, 2071. (d) Sini, G.; Sears, J. S.; Brédas, J.-L. *J. Chem. Theory Comput.* **2011**, *7*, 602.

(20) Huang, S.; Zhang, Q.; Shiota, Y.; Nakagawa, T.; Kuwabara, K.; Yoshizawa, K.; Adachi, C. *J. Chem. Theory Comput.* **2013**, *9*, 3872.

(21) (a) Becke, A. D. *J. Chem. Phys.* **1993**, *98*, 5648. (b) Stephens, P. J.; Devlin, F. J.; Chabalowski, C. F.; Frisch, M. J. *J. Phys. Chem.* **1994**, *98*, 11623.

(22) Lu, T.; Chen, F. W. *J. Comput. Chem.* **2012**, *33*, 580.

(23) Zhao, Y.; Truhlar, D. G. *J. Phys. Chem. A* **2004**, *108*, 6908.

(24) Boese, A. D.; Martin, J. M. L. *J. Chem. Phys.* **2004**, *121*, 3405.

(25) Grabowski, Z. R.; Rotkiewicz, K.; Siemiarczuk, A.; Cowley, D. J.; Baumann, W. *Nouv. J. Chim.* **1979**, *3*, 443.

(26) (a) Al-Hassan, K. A.; Saleh, N.; Abu-Abdoun, I. I.; Yousef, Y. A. *J. Incl. Phenom. Macrocycl. Chem.* **2008**, *61*, 361. (b) Koenig, M.; Bottari, G.; Brancato, G.; Barone, V.; Guldi, D. M.; Torres, T. *Chem. Sci.* **2013**, *4*, 2502.

(27) (a) Maus, M. *Photoinduced Intramolecular Charge Transfer in Donor−Acceptor Biaryls and Resulting Applicational Aspects Regarding Fluorescent Probes and Solar Energy Conversion*; Universal Publishers: Boca Raton, FL, 1998. (b) Maus, M.; Rettig, W. *Chem. Phys.* **1997**, *218*, 151. (c) Maus, M.; Rettig, W.; Jonusauskas, G.; Lapouyade, R.; Rulliere, C. *J. Phys. Chem. A* **1998**, *102*, 7393. (d) Maus, M.; Rettig, W.; Bonafoux, D.; Lapouyade, R. *J. Phys. Chem. A* **1999**, *103*, 3388. (e) Maus, M.; Rettig, W. *Chem. Phys.* **2000**, *261*, 323.

(28) (a) Davis, W. B.; Ratner, M. A.; Wasielewski, M. R. *J. Am. Chem. Soc.* **2001**, *123*, 7877. (b) Benniston, A. C.; Harriman, A. *Chem. Soc. Rev.* **2006**, *35*, 169.

(29) (a) Löwdin, P.-O. *Rev. Mod. Phys.* **1962**, *34*, 80. (b) Likhtenshtein, G. *Solar Energy Conversion: Chemical Aspects*; Wiley-VCH: Weinheim, 2012; p 25.

(30) (a) Improta, R.; Barone, V.; Scalmani, G.; Frisch, M. J. *J. Chem. Phys.* **2006**, *125*, No. 054103. (b) Improta, R.; Scalmani, G.; Frisch, M. J.; Barone, V. *J. Chem. Phys.* **2007**, *127*, No. 074504.

(31) (a) Abdel-Shafi, A. A.; Worrall, D. R. *J. Photochem. Photobiol. A: Chem.* **2005**, *172*, 170. (b) Li, B.; Nomura, H.; Miyazaki, H.; Zhang, Q.; Yoshida, K.; Suzuma, Y.; Orita, A.; Otera, J.; Adachi, C. *Chem. Lett.* **2014**, *43*, 319.
(32) Klessinger, M.; Michl, J. *Excited States and Photochemistry of Organic Molecules*; VCH, Weinheim, 1995; pp 247−260.
(33) (a) Reineke, S.; Seidler, N.; Yost, S. R.; Prins, F.; Tisdale, W. A.; Baldo, M. A. *Appl. Phys. Lett.* **2013**, *103*, No. 093302. (b) Reineke, S.; Baldo, M. A. *Sci. Rep.* **2013**, *4*, 3797.
(34) (a) Togashi, K.; Nomura, S.; Yokoyama, N.; Yasudaabc, T.; Adachi, C. *J. Mater. Chem.* **2012**, *22*, 20689. (b) Nakanotani, H.; Masui, K.; Nishide, J.; Shibata, T.; Adachi, C. *Sci. Rep.* **2013**, *3*, 2127.